Bulletin of Engineering Geology and the Environment (2021) 80:7973–7988
https://doi.org/10.1007/s10064-021-02403-2

ORIGINAL PAPER

A novel settlement forecasting model for rockfill dams based on physical causes

Chen Chen[1,2] · Xiang Lu[1,2] · Junru Li[1,2] · Jiankang Chen[1,2] · Zhengjun Zhou[3] · Liang Pei[1,2]

Received: 25 March 2021 / Accepted: 2 August 2021 / Published online: 9 August 2021

Abstract

Rockfill dams are generally constructed on thick overburden layers in mountainous and valley areas due to their high adaptability to complex geological and geographical conditions. The safety of rockfill dams is a research focus worldwide, especially with the increase of dam heights. Significant differential settlement may be induced by different embankment materials in a dam body and various stratum properties in thick overburden layers. The accurate prediction of settlement is particularly important to guarantee the serviceability and safety operation of rockfill dams. Therefore, a novel settlement forecasting model is proposed in this study. This model can achieve a successful prediction of dam settlement during the construction and operation periods. Compared with the traditional model, the settlement influential factors in the proposed model are determined based on the existing theory of coarse-grained soil deformation calculation, causing the selection of factors to have clearer physical meanings. Additionally, the geometric characteristics of the dam, the different material properties in various zones of the dam and the foundation, and the complicated external loading conditions are all considered. Then, the improved regression model for forecasting the settlement of dams is proposed. The proposed settlement forecasting model is further employed to estimate the deformation of a high rockfill dam in China. The results prove that this novel method shows high accuracy and agrees well with the monitoring consequences, and this method is superior to the traditional statistical regression model in predicting dam settlement during the construction period.

Keywords Rockfill dam · Settlement · Physical causes · Forecasting model · Statistical regression model

Introduction

Various types of dams have been increasingly constructed all over the world for hydropower generation, flood control, irrigation, and water supply. However, with the exploitation and exhaustion of natural satisfactory dam sites, many new dams have had to be constructed in adverse conditions; facing problems such as thick overburden layers, complex topographical, and geological conditions; high seismic intensity areas; and inconvenient transportation routes. In this type of harsh natural environment, rockfill dams are one of the most promising dam types due to their excellent adaptability to diverse geological and geographical conditions, full utilization of local materials, and low construction costs.

At present, there are more than 600 rockfill dams around the world, and China possesses the largest number of these dams (Ma and Chi 2016). Some of the typical rockfill dams that have been recently constructed in China are listed in Table 1. Challenges can be found in both the height of these dams and the thickness of the overburden layers. With the increasing dam height, the internal stress within the dam is high, the stress is distributed within the various zones or layers within the embankment, and the foundation is complicated, making an accurate prediction of the dam deformation even more difficult.

Dam deformation is the nonlinear behavior caused by the coupling action of multiple random factors (such as the time, weight of the dam, water pressure, and temperature effect) and it has been widely discussed in fields such as earth dams, slopes, and landslides (Herrera et al. 2009;

✉ Xiang Lu
2017323060042@stu.scu.edu.cn

1 State Key Laboratory of Hydraulics and Mountain River Engineering, Sichuan University, Chengdu 610065, China

2 College of Water Resource & Hydropower, Sichuan University, No. 24 South Section 1, Yihuan Road, Chengdu 610065, China

3 PowerChina Chengdu Engineering Corporation Limited, Chengdu 610072, China

Table 1 Typical rockfill dams constructed in China

No	Name	Location	Finish time	H_{max} (m)	T_{max} (m)	Reference
1	Xiaolangdi	Huanghe Basin, Henan Province	2000	160	80	Li (2009)
2	Qiaoqi	Baoxing River Basin, Sichuan Province	2006	125.5	72	Feng et al. (2019)
3	Shuiniujia	Fujiang River Basin, Sichuan Province	2006	108	30	Zhu and Zhou (2010)
4	Yele	Nanya River Basin, Sichuan Province	2006	124.5	420	Wang et al. (2010)
5	Shiziping	Min River Basin, Sichuan Province	2010	136	101.8	Zhang et al. (2016)
6	Pubugou	Dadu River Basin, Sichuan Province	2010	186	75	Xue et al. (2012)
7	Maoergai	Heishui River Basin, Sichuan Province	2011	147	57	Feng et al. (2019)
8	Luding	Dadu River Basin, Sichuan Province	2011	84	148	Jiang et al. (2011)
9	Nuozhadu	Lancang River Basin, Yunnan Province	2014	261.5	30	Dong et al. (2012)
10	Houziyan	Dadu River Basin, Sichuan Province	2016	223.5	70	Xiang and Hu (2016)
11	Huangjinping	Dadu River Basin, Sichuan Province	2016	85.5	133.92	Wan and He (2016)
12	Changheba	Dadu River Basin, Sichuan Province	2018	242.5	79.3	Wu and Shui (2019)

H_{max}, the maximum dam height; T_{max}, the maximum thickness of the overburden

Macfarlane 2009; Tomás et al. 2013; Rashidi and Haeri 2017; Alnedawi et al. 2019; Yu et al. 2020). Regression analysis has been widely used to forecast dam deformation in previous research, but for this type of analysis, the adopted influential factors can seriously affect the prediction performance. The selection of influential factors for the commonly used regression models includes prior knowledge, linear correlation coefficients, multiple linear regression, principal component analysis, the gray correlation analysis method, partial mutual information, cluster analysis, and neural networks. The advantages and shortcomings of some normally used methods for selecting influential factors of dam deformation models are listed in Table 2 (Chen et al. 2010; Yu et al. 2010; Yao et al. 2011; Kan et al. 2015; Han et al. 2020). Most of the traditional regression models are mainly composed of factors of the environmental variables (such as water level, temperature, and rainfall), time effect, and dam height, which place less emphasis on the effects of the foundation geological conditions and material properties in different dam zones (Sortis and Paoliani 2007; Léger and Leclerc 2007; Mata et al. 2014). Additionally, the selection of influential factors is mainly based on previous experience, a large quantity of monitoring data, and mathematical calculations without

Table 2 Main selection of influential factors in the regression model

Method	Basic principles	Parameters	Advantages	Shortcomings
Prior knowledge	Using experience and knowledge	/	Convenient	Relying excessively on experience
Linear correlation coefficient	Using simple linear correlation of variables	Correlation coefficient	Simple and accurate	Ignoring the nonlinear relationship of variables
Multiple linear regression	Using the significance degree of variables	*F*-test of significance	Less computation	Only one set of regression factors can be identified
Principal component analysis	Using the contribution index	Characteristic value	Avoiding the influence of factor correlation	Poor accuracy when the factor collinearity is poor
Gray correlation analysis	Using the gray relational grade among variables	Gray correlation coefficient	Avoiding the influence of insufficient original information	No clear evaluation index to select factors
Partial mutual information	Using the significance degree of variables	Hampel test of significance	Removing the irrelevant variables	Relying on the discrete data
Cluster analysis	Using the similarity relationship of variables	Similarity degree	Displaying the differences of variables intuitively	Cumbersome calculation when the factor combination is too much
Neural network	Using the correlation between the dependent and independent variables	Correlation coefficient	Mapping any complex nonlinear relationship	Cumbersome calculation when the factor combination is too much

very clear criteria for the physical causes of dam deformation. However, even for two dams with similar heights, crest lengths and alluvium overburden thickness can exhibit completely different deformation patterns (Feng et al. 2020), which indicates that the imperfect selection criteria and neglection of important factors will lead to significant differences in dam deformation prediction. The deformation calculated by the theory of soil deformation is closely related to the material properties and structure characteristics, and the influential factors determined by the theory of soil deformation can better represent the relationship between dam deformation and internal characteristics.

Recently, with the development of artificial intelligence (AI) technology, some new models have been proposed for dam deformation predictions, such as artificial neural network models, gray models, and time series models (Gurbuz 2011; Tasci and Kose 2016; Behnia et al. 2016; Nie et al. 2017; Salazar et al. 2017; Zou et al. 2018; Kim and Kim 2018; Zhang et al. 2019; Li and Wang 2019; Gu et al. 2020; Lawal and Kwon 2021; Liu et al. 2021). Kim and Kim (2018) established a neural network model for the prediction of the relative crest settlement of concrete-faced rockfill dams. Su et al. (2018) established a prediction model of dam deformation combined with a support vector machine, phase space reconstruction, wavelet analysis, and particle swarm optimization. Although these models performed with high accuracy, most of them were developed based on a mathematical algorithm without consideration of physical and mechanical causes that induce dam settlement (Niu et al. 2019), particularly for rockfill dams, which are generally divided into several zones with different materials and constructed with harsh geological conditions such as thick overburden layers. The materials with various physical and mechanical properties in the dam body and the foundation may induce significant differential settlements, which threatens the serviceability and safety operation of a dam.

Therefore, a novel settlement forecasting model is proposed in this study that evaluates dam deformation from the perspective of its physical mechanism, which is the deformation caused by the dam body and the foundation. The proposed method can successfully achieve the prediction of dam settlement during both the construction and operation periods. The physical and mechanical properties of materials in the different zones of a rockfill dam and the foundation, the complexity of the geological conditions, and the dam geometric characteristics are all considered. A detailed introduction and comparison of the developed settlement forecasting model and the traditional regression models are presented first, followed by a case study of the PB high rockfill dam to verify the high accuracy and advantages of the proposed method.

Traditional regression model

Dam behavior has strong interactions with boundary conditions such as water level, rainfall, and temperature (Hampel 1974). The monitoring period of dam deformation can be generally divided into two stages: the construction period and the operation period. The deformation characteristics in the two stages are different due to the loading conditions and environmental factors.

During the construction period, the temperature in a dam remains stable, which has little effect on the internal deformation of the dam. Therefore, the types of regression statistical models of settlement can be expressed as (Tang et al. 2001):

$$S = \begin{cases} a_0 + b_0 {h_i}^{a_0}\left(c_0 - e^{-\beta_0 t}\right) & (A) \\ a_1 + b_1 {h_i}^{a_1} + c_1 \lg\left(1 + \beta_1 t\right) & (B) \\ f(t) & (C) \end{cases}, \tag{1}$$

where S is the total settlement; h_i is the vertical distance between point i and the filling dam crest; t is the time in the day from the beginning of the analysis; a_i, b_i, α_i, c_i, and β_i $(i = 0,1)$ are the undetermined coefficients; and $f(t)$ is the curve function of time. Power exponential, hyperbola, exponential, and logarithmic curves are the commonly used functions in the regression statistics of settlement. In this research, a multivariate nonlinear regression (MNR) model in the form of (A) in Eq. (1) is adopted, in which the regression coefficients are solved based on the least square method.

During the operation period, the deformation is mainly affected by the hydrostatic pressure, temperature, and time effect, and thus, the hydrothermal time (HTT) model (Léger and Leclerc 2007; Mata et al. 2014) is selected and the deformation y can be written as:

$$y = y_H + y_T + y_t + c, \tag{2}$$

where c is a constant and y_H, y_T and y_t are the contributions due to the elastic effect of hydrostatic pressure, temperature, and the effect function of time. The functional forms are normally considered to be (Sortis and Paoliani 2007; Mata et al. 2014; Prakash et al. 2018):

$$y_H = \sum_{i=1}^{3} a_{1i} {H_1}^i + \sum_{i=1}^{3} a_{2j} {H_2}^j, \tag{3}$$

$$y_T = \sum b_i T_i, \tag{4}$$

$$y_t = c_1 t + c_2 \ln t, \tag{5}$$

where a_{1i}, a_{2j}, b_i, c_1, and c_2 are the regression coefficients, H_1 and H_2 are the heights of the water in the reservoir and downstream, T_i is the recorded temperature, and t is the time of day at the beginning of the analysis.

A novel settlement forecasting model based on physical causes

Model of settlement during the construction period

The settlement of a rockfill dam on overburden layers during the construction period consists of the immediate settlement deformation caused by filling and the creep settlement with time.

Immediate settlement

Generally, the immediate settlement in an arbitrary point of a dam is composed of the compressive deformation of the dam body and the associated deformation of the dam foundation, which can be presented as:

$$S_i = S_{\mathrm{d}i} + S_{\mathrm{l}i}, \tag{6}$$

where S_i is the immediate settlement of point i, S_{di} is the compressive deformation of the dam body, and S_{li} is the associated deformation of the dam foundation.

Figure 1 shows a simplified cross-section of an embankment dam (Dam height: H) with point i. Based on the position relationship, the compressive deformation S_{di} can be calculated as:

$$S_{\mathrm{d}i} = \int_0^{H-z}\int_0^{z}\frac{\alpha\gamma}{E_s}dz_1dz_2, \tag{7}$$

with

$$E_s = k_e P_a\left(\frac{\sigma_3}{P_a}\right)^n\left(1 - R_f\frac{(\sigma_1-\sigma_3)(1-\sin\varphi)}{2c\cos\varphi + 2\sigma_3\sin\varphi}\right)^2, \tag{8}$$

$$\begin{aligned}\sigma_1 &= \beta\gamma z\\ \sigma_3 &= \eta\gamma z\end{aligned}, \tag{9}$$

where a is the correction coefficient of the compressive stress, γ is the bulk density of the materials, z_1 and z_2 are the integration variables, E_s is the compressive modulus, k_e and R_f are the experiment constants, P_a is the atmospheric pressure, c is the cohesion of the soil, φ is the friction angle of the soil, σ_1 and σ_3 are the major and minor principal stresses, and β and η are the coefficients of the axial and confining stresses of the soils in the dams, respectively.

The compressive deformation S_{di} can then be deduced based on the Duncan-Chang model:

$$\begin{aligned}S_{di} &= \int_0^{H-z}\int_0^{z}B\left(z_1+z_2\right)^{-n}dz_1dz_2 = \frac{B}{(1-n)(2-n)}\\ &\left(H^{2-n} - z^{2-n} - (H-z)^{2-n}\right) = \frac{B}{(1-n)(2-n)}f_d,\end{aligned} \tag{10}$$

with

$$B = \alpha\gamma^{1-n}/\left(k_e p_a\left(\eta/p_a\right)^n A\right), \tag{11}$$

$$A = 1 - R_f(\beta-\eta)(1-\sin\varphi)/(2\eta\sin\varphi), \tag{12}$$

where z is the vertical distance between point i and the dam foundation surface; n is the parameter in the Duncan-Chang model used in dams; f_d is the power function of the dam height for settlement deformation; and the other symbols have the same meaning as before.

The influence of the overburden layers on the dam deformation is defined as the associated deformation S_{li}, and this can be expressed by:

$$\begin{aligned}S_{li} &= \int_0^{H-z}\int_0^{z}\frac{\alpha\gamma}{E_s}dz_1dz_2 = \frac{B_l}{\left(1-n'\right)\left(2-n'\right)}\\ &\left[\left(H_1+H-z\right)^{2-n'} - H^{2-n'} - (H-z)^{2-n'}\right]\\ &= \frac{B_l}{\left(1-n'\right)\left(2-n'\right)}f_1,\end{aligned} \tag{13}$$

with

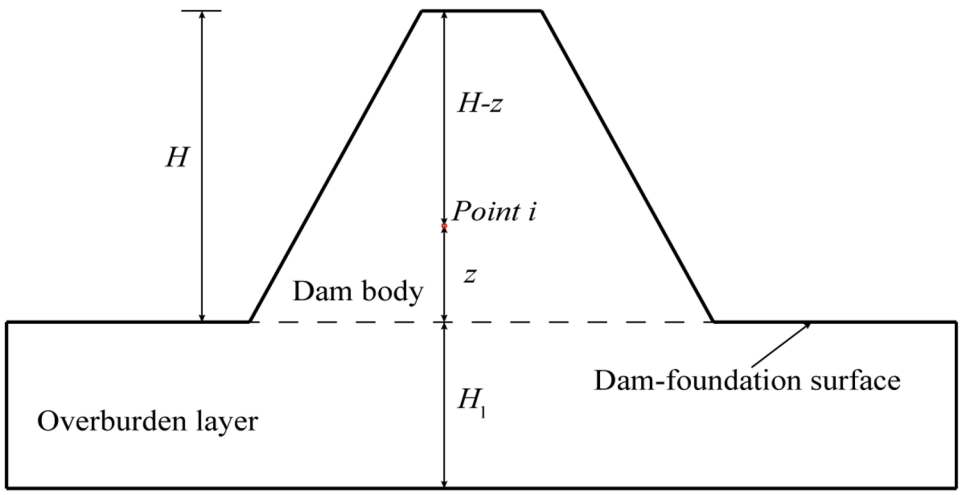

Fig. 1 Position relationship of point *i*

$$B_1 = \phi\alpha_1\gamma^{1-n'} / \left(k_e p_a \left(\eta_l / p_a\right)^{n'} A_1 \right), \tag{14}$$

$$A_1 = 1 - R_f\left(\beta_1 - \eta_1\right)(1 - \sin\varphi) / \left(2\eta_1 \sin\varphi\right), \tag{15}$$

where β_1 and η_1 are the coefficients of the principal stress of the soils in the foundation, f is the power function of the overburden layer depth for settlement deformation, n' is the parameter in the Duncan-Chang model used in the foundation, ϕ is the diffusion coefficient of the stress in the dam foundation, and H_1 is the depth of the overburden layer.

Therefore, the immediate deformation S_i of an arbitrary point i can be obtained based on Eqs. (10) and (13).

Figure 2 further shows the settlement results of a homogeneous earth rock dam induced by the dam body and foundation using the promoted model and the numerical simulation method, in which FLAC-3D software is applied in this research. The height of the dam is 100 m, and the height of the overburden layer is 50 m. More details can be seen in Fig. 1. It can be found that the laws of settlement revealed by f_d (the power function of dam height for settlement deformation) and f_1 (the power function of overburden layer depth for settlement deformation) are consistent with those obtained with FLAC-3D, implying that the abovementioned formulas based on the physical and mechanical causes of dam settlement during the construction period are reasonable.

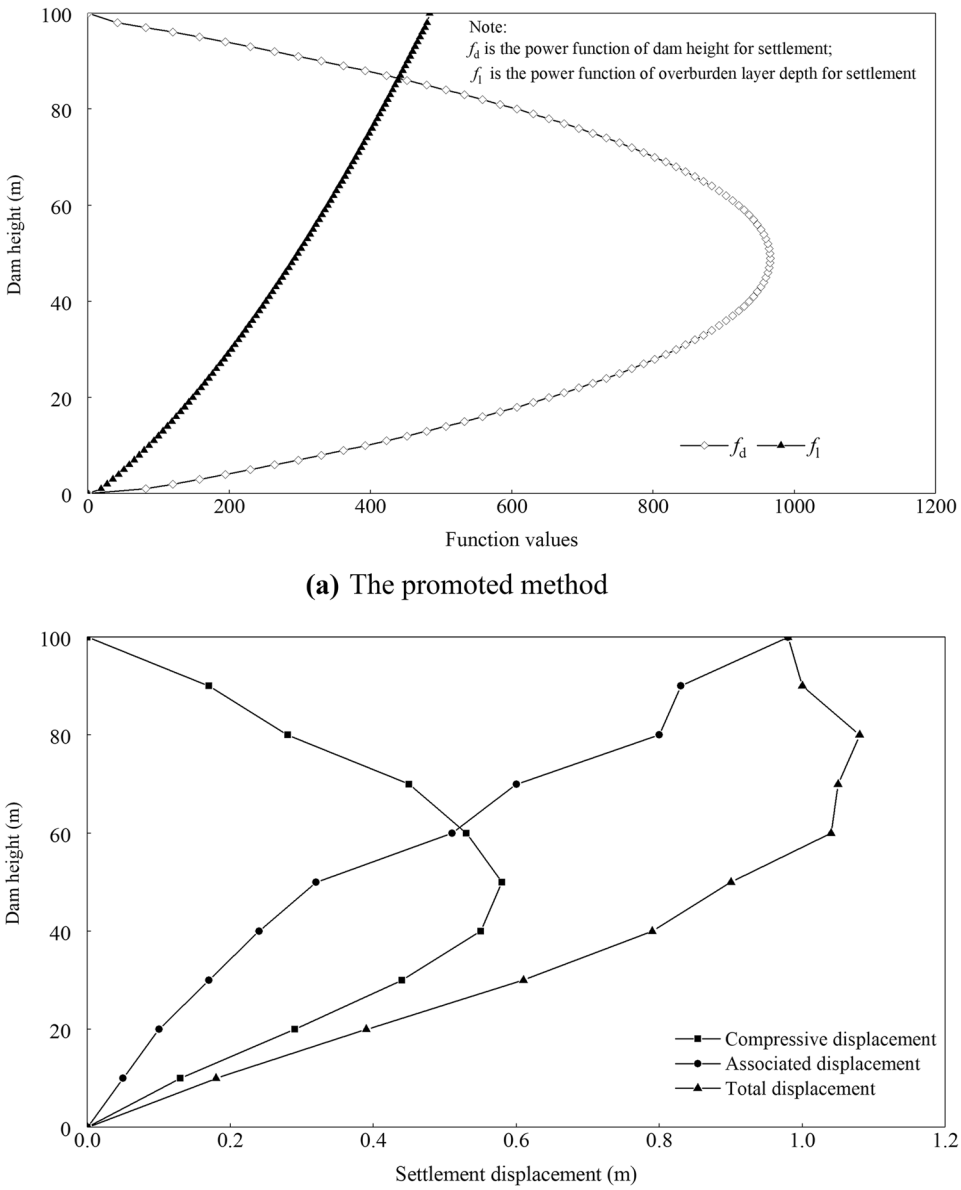

(a) The promoted method

(b) Settlement calculated with FLAC-3D

Fig. 2 Laws for the settlement deformation with the dam height

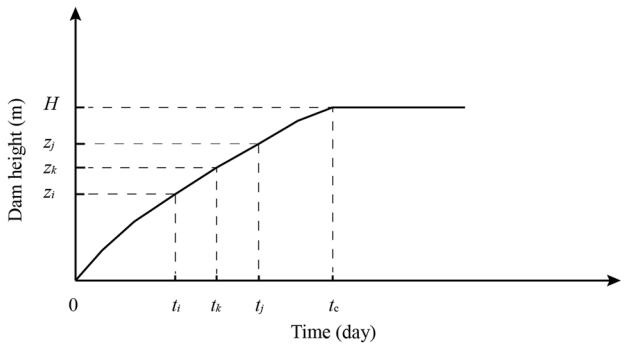

Fig. 3 The relationship between the dam height and time

Creep settlement

Generally, the creep strain ε_t can be obtained with the empirical creep model as (Qian and Yin 1995):

$$\varepsilon_t = \varepsilon_f\left(1 - e^{-\alpha t}\right), \tag{16}$$

where ε_f is the total creep strain, α is the constant of the exponential decay curve, and t is the time.

In the triaxial creep test, the ultimate axial creep strain ε_{Lf} has a specific relationship with the ultimate volumetric creep strain ε_{Vf} and the ultimate shear creep strain ε_{Sf}, which can be expressed as (Shen 1994; Li et al. 2004a, 2004b):

$$\varepsilon_{\mathrm{Lf}} = \frac{1}{3}\varepsilon_{\mathrm{Vf}} + 2\varepsilon_{\mathrm{Sf}}, \tag{17}$$

$$\varepsilon_{\mathrm{Vf}} = b\left(\frac{\sigma_3}{Pa}\right)^{m_1} + c\left(\frac{q}{Pa}\right)^{m_2}, \tag{18}$$

$$\varepsilon_{\mathrm{Sf}} = d\left(\frac{S_{\mathrm{L}}}{1 - S_{\mathrm{L}}}\right)^{m_3}, \tag{19}$$

where b, c, d, m_1, m_2, and m_3 are the material parameters of the creep, σ_3 is the confining pressure, qq is the deviatoric stress, and S_L is the stress level, which can be theoretically represented as:

$$S_{\mathrm{L}} = \frac{(\sigma_1 - \sigma_3)(1 - \sin\varphi)}{2c\cos\varphi + 2\sigma_3\sin\varphi}. \tag{20}$$

Therefore, the ultimate axial creep strain ε_{Lf} is given by:

$$\varepsilon_{\mathrm{Lf}} = \frac{1}{3}\left[b\left(\frac{\sigma_3}{Pa}\right)^{m_1} + c\left(\frac{q}{Pa}\right)^{m_2}\right] + 2d\left(\frac{S_L}{1 - S_L}\right)^{m_3}. \tag{21}$$

Equation (21) can be rewritten in the following form:

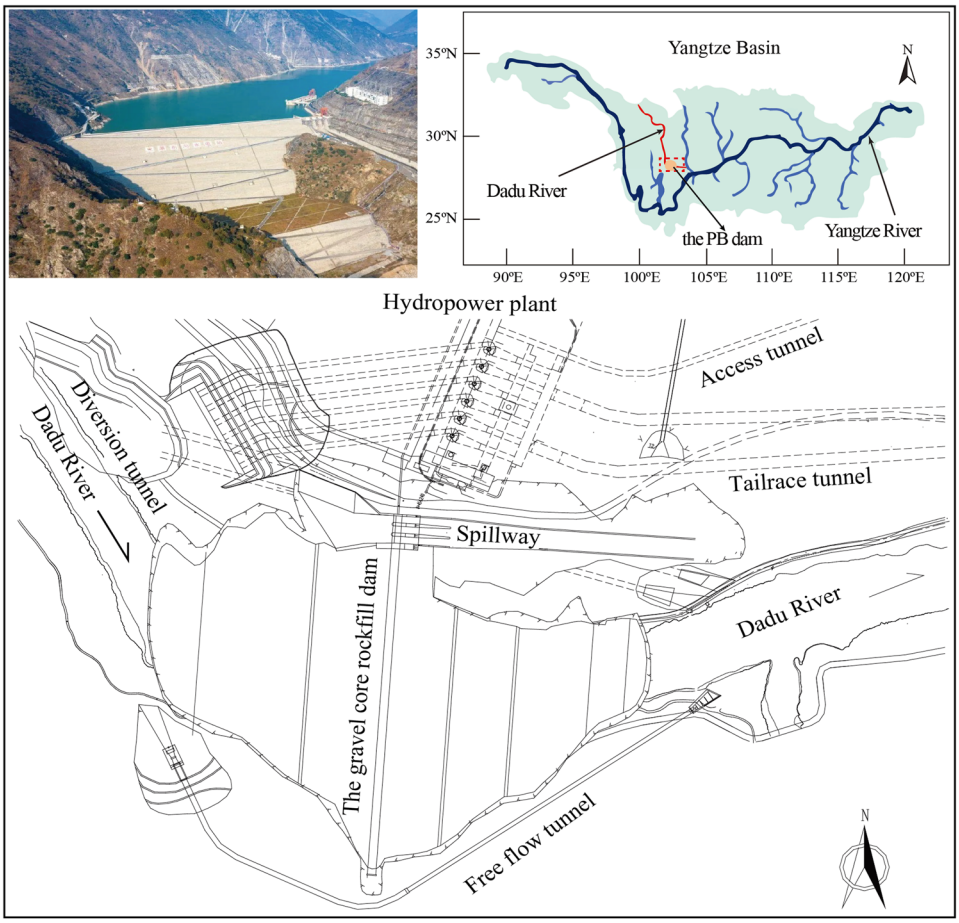

Fig. 4 The layout of the PB hydropower station

$$\varepsilon_{\mathrm{Lf}} = C_1 z^{m_1} + C_2 z^{\frac{m_2}{2}} + D, \tag{22}$$

with

$$C_1 = \frac{b}{3}\left(\frac{\eta\gamma}{p_a}\right)^{m_1}, \tag{23}$$

$$C_2 = \frac{\left(2\left((\beta-\eta)^2+(\beta-\lambda)^2+(\eta-\lambda)^2\right)\gamma\right)^{\frac{m_2}{2}}}{6{p_a}^{m_2}}, \tag{24}$$

$$D = 2d\left[\frac{(\beta-\eta)(1-\sin\varphi)}{(\beta+\eta)\sin\varphi-(\beta-\eta)}\right]^{m_3}, \tag{25}$$

where z is the depth of the soils, λ is the coefficient of the intermediate principal stress, and the other symbols have the same meaning as before.

Figure 3 shows the relationship between the filling height and the time, in which t_c is the total filling time, t_i, t_j, and t_k are the times of finishing the ith, jth, and kth fillings ($i < k < j$, and the maximum of j is N). The cumulative settlement induced by creep within a dam height of z_j can be obtained as:

$$S_{zj} = \int_0^{z_j} \Delta\varepsilon_i\left(e^{-\alpha(t_j-t_i)} - e^{-\alpha(t_c-t_i)}\right)\mathrm{d}z. \tag{26}$$

The creep incremental strain $\Delta\varepsilon_i$, which stands for the effect of the kth filling on the creep-induced settlement of the ith layer below can be defined based on Eq. (16):

$$\begin{aligned}\Delta\varepsilon_i = & f_k(z_i) = C_1\left[\left(z_k - z_i\right)^{m_1} - \left(z_{k-1} - z_i\right)^{m_1}\right] \\ & + C_2\left[\left(z_k - z_i\right)^{\frac{m_2}{2}} - \left(z_{k-1} - z_i\right)^{\frac{m_2}{2}}\right] + D.\end{aligned} \tag{27}$$

Then, the creep incremental deformation in any filling layer can be obtained as:

$$\begin{aligned}S_{zj} &= \int_0^{z_j} \Delta\varepsilon_i\left(e^{-\alpha(t_j-t_i)} - e^{-\alpha(t_c-t_i)}\right)\mathrm{d}z \\ &\approx \sum_{i=1}^{j}\sum_{k=i+1}^{N} \Delta\varepsilon_i\left(e^{-\alpha(t_j-t_i)} - e^{-\alpha(t_c-t_i)}\right) \\ &= \Delta z_i\left(\sum_{i=1}^{j} a_i e^{-\alpha(t_j-t_i)} - \sum_{i=1}^{j} a_i e^{-\alpha(t_c-t_i)}\right),\end{aligned} \tag{28}$$

where a_i is the intermediate variable.

Thus, the ultimate creep deformation of a dam is given by:

$$S_z = \sum_{i=1}^{j} S_{zj} = \sum_{i=1}^{j} K_i z\left(e^{-\alpha(t_j-t_i)} - e^{-\alpha(t_c-t_i)}\right), \tag{29}$$

where K_i is the constant coefficient and z is the vertical distance between the point and the dam foundation surface.

Finally, the total settlement of a dam during the construction period can be calculated as:

$$S = S_{\mathrm{d}} i + S_1 i + S_z + S_{z0}, \tag{30}$$

where S_{z0} is the creep of the overburden layer.

Model of settlement during the operation period

After the completion of dam construction and filling, the settlement of a rockfill dam mainly consists of the wetting deformation caused by impounding and the unfinished creep deformation during the construction period, namely

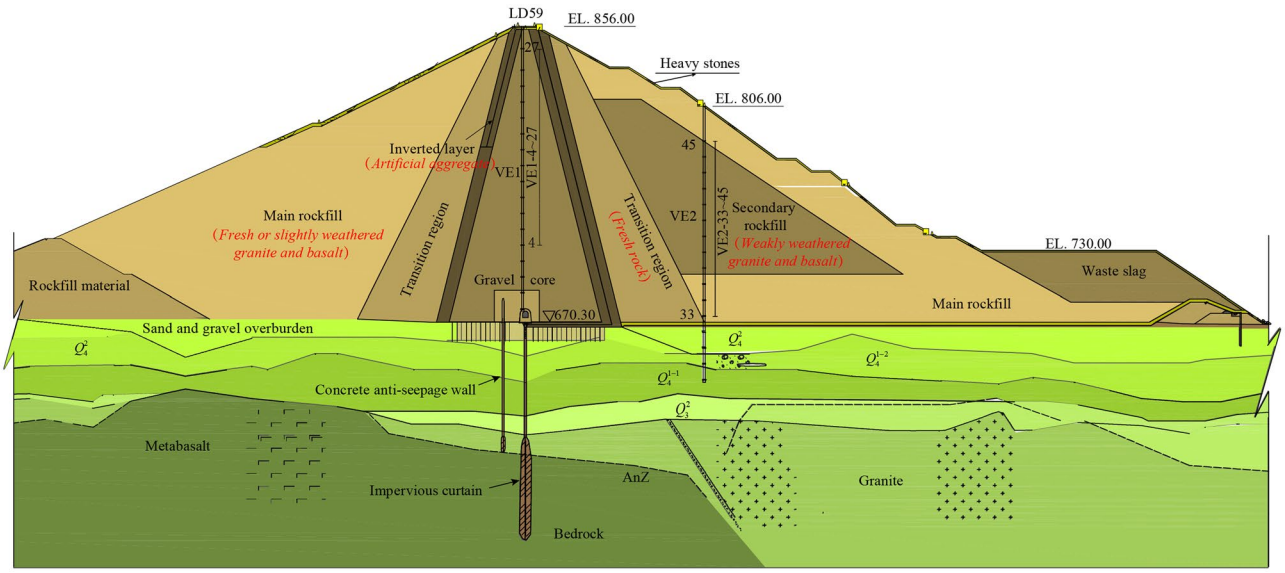

Fig. 5 Typical section of the PB hydropower station

Table 3 Specific information for monitoring points

Points	Elevation (m)	Starting data	Points	Elevation (m)	Starting data
VE1-4	718.920	2007/12/18	VE1-22	819.458	2009/05/04
VE1-5	734.651	2008/02/13	VE1-23	824.764	2009/05/16
VE1-6	741.134	2008/03/06	VE1-24	829.834	2009/06/05
VE1-7	744.574	2008/04/13	VE1-25	833.718	2009/06/26
VE1-8	749.096	2008/05/02	VE1-26	839.354	2009/08/17
VE1-9	752.800	2008/05/07	VE1-27	842.020	2009/08/17
VE1-10	755.912	2008/06/14	VE2-33	673.057	2007/04/21
VE1-11	759.358	2008/07/05	VE2-34	683.816	2007/07/15
VE1-12	762.648	2008/07/24	VE2-36	703.901	2007/11/17
VE1-13	767.037	2008/09/06	VE2-37	713.468	2007/11/24
VE1-14	772.388	2008/11/08	VE2-38	722.408	2008/01/12
VE1-15	776.634	2008/11/15	VE2-39	735.629	2008/01/22
VE1-16	782.331	2008/12/04	VE2-40	745.764	2008/04/19
VE1-17	788.394	2008/12/24	VE2-41	756.204	2008/06/12
VE1-18	794.425	2009/01/17	VE2-42	761.039	2008/06/19
VE1-19	801.075	2009/02/20	VE2-43	771.089	2008/08/12
VE1-20	806.690	2009/03/20	VE2-44	778.591	2008/09/11
VE1-21	813.632	2009/04/14	VE2-45	786.213	2008/09/18

$$S' = S'_w + S'_z, \tag{31}$$

where S' is the settlement, S'_w is the wetting deformation, and S'_z is the unfinished creep deformation during the construction period.

During the initial operation period, the rockfill area and the core wall at the upstream side will be saturated or wetted by water, causing collapse deformation. The value of the collapse deformation is closely related to the physical and mechanical properties of the embankment materials and the initial water level. Based on the modified Shen Zhu-jiang's wetting deformation model (Li and Liu 1998), the wetting-induced volume deformation and shear deformation can be expressed as:

$$\Delta\varepsilon_{\mathrm{v}}^{w} = C_w\left(\frac{\sigma_3}{Pa}\right)^{n_w}, \tag{32}$$

$$\Delta\gamma^{w} = D_w\frac{S_{\mathrm{L}}}{1-S_{\mathrm{L}}}, \tag{33}$$

where $\Delta\varepsilon_v^w$ and $\Delta\gamma^w$ are the wetting-induced volume deformation and the shear deformation, respectively, and C_w, D_w, and n_w are the constant parameters of the materials.

Then, the total wetting stress can be obtained based on the Prandtl-Reuss flow rule (Li et al. 2005):

$$\{\Delta\varepsilon\} = \frac{[I]}{3}\Delta\varepsilon_{\mathrm{v}}^{w} + \frac{\{S\}}{q}\Delta\gamma^{w}, \tag{34}$$

where $\{\Delta\varepsilon\}$ is the strain tensor, $\{S\}$ is the deviatoric stress vector, $[I]$ is the identity matrix, and q is the generalized shear stress.

Consequently, the settlement of the embankment materials in a rockfill dam can be expressed as:

$$S'_w = \begin{cases} \psi z + \frac{\varsigma}{1+n_w}\left[H^{1+n_w} - (H-z)^{1+n_w}\right] & z \le H_w \\ \psi H_w + \frac{\varsigma}{1+n_w}\left[H^{1+n_w} - \left(H-H_w\right)^{1+n_w}\right] & z > H_w \end{cases}, \tag{35}$$

where H is the height of the monitoring point, H_w is the height of the water level in the monitoring point, and ς and ψ are parameters to be solved through the least square method.

Moreover, the creep deformation after the construction period can be calculated at the time of completion of the dam construction and filling, namely, the time t_c in Fig. 3. Therefore, the settlement of a rockfill dam during the initial operation period can be calculated using Eq. (29) with the beginning time of t_c and Eq. (35).

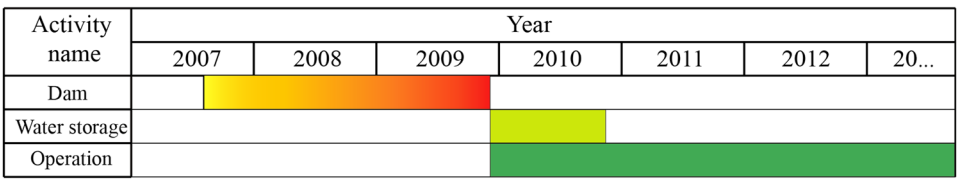

Fig. 6 The time span of the construction and operation periods of the PB dam

Table 4 The multi-correlation coefficients of the models during the initial operation period

Points	20	21	22	23	24	25	26	27	LD59
HTT	0.959	0.969	0.976	0.966	0.981	0.982	0.985	0.986	0.994
This research	0.965	0.971	0.975	0.978	0.980	0.983	0.984	0.981	0.985

Case study

Project specification

The PB hydropower station is located on the Dadu River on the border between Hanyuan County and Ganluo County, Sichuan Province, China. This enormous hydroelectric project has a total electric generating capacity of 3600 MW and the ability to seasonally regulate output. The storage capacity is 5.39 billion m^3, the maximum height of the dam is 186 m, and the normal water storage level is 850 m. The maximum thickness of the foundation overburden layer is 77.9 m. The hydropower station is mainly composed of three parts: a gravel soil core rockfill dam, a waterpower generation system, and a discharge structure (Fig. 4).

As shown in Fig. 5, from the upstream side to the downstream side of the dam, the rockfill materials are divided into the upstream main rockfill region, transition region, inverted layer, gravel core, inverted layer, transition region, downstream secondary rockfill region, and downstream main rockfill region. The stratum lithology at the dam site is mainly composed of the shallow metamorphic basalt of the pre-Sinian system, the rhyolitic tuff of the Sinian system, and the coarse-grained granite of the Chengjiang system. The overburden of the dam foundation can be divided into four layers: the floated boulder and pebble layer $\left(Q_3^2\right)$ the pebble and gravel layer $\left(Q_4^{1-1}\right)$, the pebble layer with the boulder layer $\left(Q_4^{1-2}\right)$ and the boulder and pebble layer $\left(Q_4^2\right)$.

An integrated monitoring system is installed inside the dam to measure the settlement. Figure 5 shows the layout of the settlement points and the geological condition of Sect. 0 + 240 m. Two groups of settlement rings named VE1–VE2 are adopted, which consist of 20 and 13 monitoring points numbered VE1-4–23 and VE2-33–45, respectively. Other information about the monitoring points is listed in Table 3, and the time spans of the construction and operation periods of the PB rockfill dam are shown in Fig. 6.

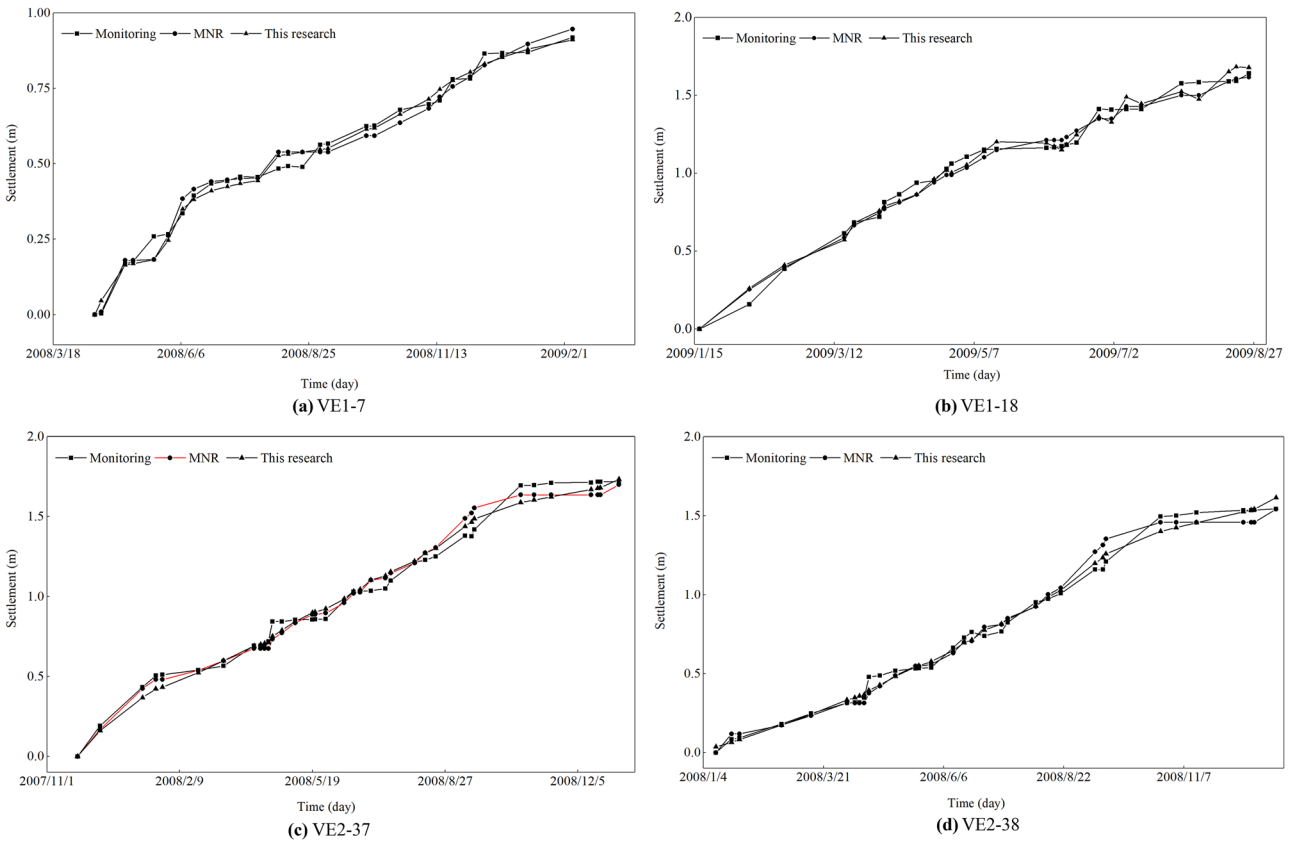

Fig. 7 Prediction results for the typical monitoring points during the construction period

Results and analysis

According to the model of settlement during the construction period (Eq. (30)) and that during the initial operation period (Eq. (35)), the prediction statistical regression models of settlement based on physical causes are established, and the coefficients to be solved are determined with the least square method using the monitoring data, which is also introduced for the solution of the traditional statistical regression model. Table 4 shows the multi-correlation coefficient of the two models during the initial operation period. Initially, the multi-correlation coefficients of the two regression models are all above 0.95, which indicates that the fitting effect is good. A detailed comparative analysis of the proposed method and the traditional method is shown below.

Settlement during the construction period

The monitoring data for VE1 and VE2 in Sect. 0+240 during the construction period are selected to build the traditional MNR model and the proposed model in this research. Some of the typical results are shown in Fig. 7. It can be found that although both of the methods can describe the diachronic process of dam settlement well, the promoted forecasting model performs with better accuracy. The monitoring point of VE1-18 is taken as an example, and when using the MNR model, the maximum relative error is 8.1% on the date of April 14, 2009, while the minimum relative error is 0.03% on Aug. 17, 2009. Nevertheless, the maximum and minimum relative errors are reduced to 5.61% and 0.01% by using the proposed forecasting model. Since the accuracy of the MNR model strongly depends on the reliability and length of the monitoring data, the predicted results of settlement for VE1 with more monitoring points display a better law than that for VE2.

The indexes of the average relative error δ and the mean square error (MSE) are adopted to verify the accuracy of the method, and these indexes can be calculated as shown below:

$$\delta = \frac{|y_i - \hat{y}_i|}{y_i} \times 100\%, \tag{36}$$

$$MSE = \sqrt{\frac{\sum_{i=1}^{n} (y_i - \hat{y}_i)^2}{n}}, \tag{37}$$

where y_i is the measured value, $\hat{y}_i$ is the calculated value for the models, and n is the number of measured values.

The average relative errors and MSEs of the points in VE1 and VE2 are shown in Fig. 8. The results illustrate the

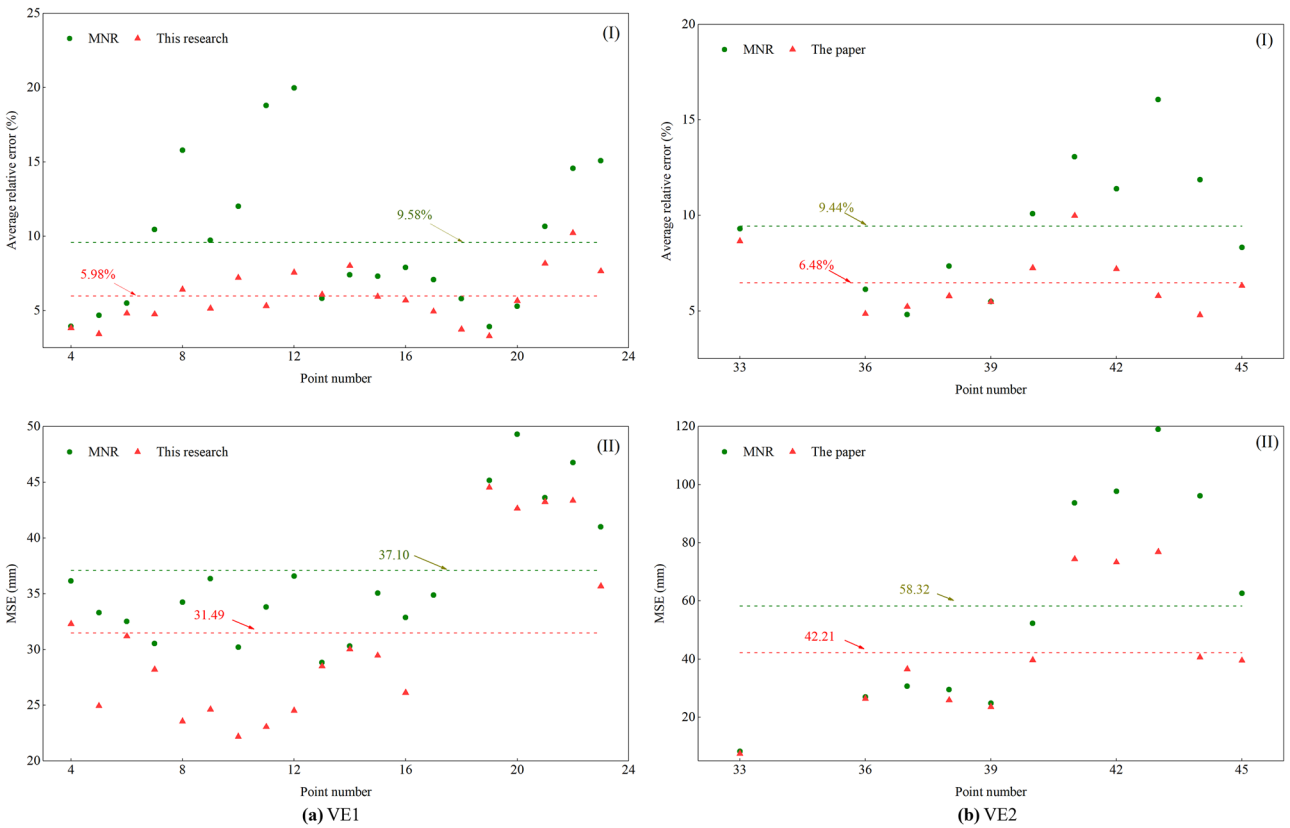

Fig. 8 Average relative errors and MSE of results during the construction period

fact that the average relative error of every single point at different altitudes varies. Using the proposed method, the average relative errors of all points in VE1 and VE2 are 5.98% and 6.48%, respectively, which is significantly lower than the values obtained with the traditional MNR method at 9.58% and 9.44%, respectively. Additionally, the MSE of the proposed method was smaller than that of the traditional method. The results prove the validity of the proposed model, which agrees well with the monitoring data and performs with higher accuracy than the traditional MNR method to forecast dam settlement during the construction period.

Settlement during the initial operation period

The monitoring data for VE1 and LD59 (at the dam crest) in Sect. 0 + 240 during the initial operation period are selected to build the traditional HTT model and the proposed model in this research. The results of the relative error, MSE, and the development of the dam settlement over time using the two methods are shown in Table 5 and Figs. 9 and 10. It can be found that the average relative error of the results obtained with the HTT method is between 1.19 and 3.52% and that predicted by the proposed method is between 1.02 and 4.48%. For both of the two methods, the maximum average relative errors can be found at the point of VE1-27, while the minimal average relative errors occur at the point of VE1-20, indicating that the precision of the two methods slightly decreases with the increase of the dam height.

The accuracy of some points using the proposed method is slightly lower than that of the traditional method. For example, the maximum and average relative errors of LD59 are 9.43% and 3.31%, respectively, which are higher than those of the HTT model. Although the maximum relative error of VE1-27 using the proposed method is lower than that of the traditional method, the average relative error and the MSE are higher. It is noted that the average relative errors of both methods are all smaller than 5%, indicating that the accuracy of these methods meets the engineering requirements.

Discussion

The results show that the average relative errors of the settlement obtained during the initial operation period are smaller than those obtained during the construction period when using either the traditional MNR (HTT) method or the method proposed in this paper. This may be because the regularity of the settlement sequences during the initial operation period is better than that during the construction period, which is less affected by external environmental factors.

Table 5 Relative errors of the prediction results during the initial operation period

Relative error	VE1-20		VE1-21		VE1-22		VE1-23		VE1-24		VE1-25		VE1-26		VE1-27		LD59	
Method	HTT	This research	HTT	This research	HTT	This research	HTT	This research	HTT	This research	HTT	This research	HTT	This research	HTT	This research	HTT	This research
Max	3.26%	3.81%	4.80%	4.93%	3.60%	4.02%	9.26%	6.68%	5.37%	5.49%	6.12%	6.64%	10.89%	7.44%	15.09%	8.11%	8.91%	9.43%
Min	0.01%	0.01%	0.04%	0.01%	0.00%	0.01%	0.06%	0.02%	0.01%	0.02%	0.00%	0.02%	0.01%	0.01%	0.01%	0.36%	0.00%	0.24%
Aver	1.19%	1.02%	1.22%	1.32%	1.31%	1.25%	1.64%	1.75%	1.70%	2.01%	2.15%	2.54%	2.76%	2.93%	3.52%	4.48%	1.28%	3.31%

Compared with the traditional method, the accuracy advantage of the proposed method is more obvious during the construction period. The reason for this may be that the main influential factor during the construction period is the filling height, which is better quantified in the method proposed in this paper; that is, the proportion of the filling component (immediate settlement) in the settlement displacement is relatively high (as seen in Fig. 11).

However, the accuracy advantage of the proposed method is not obvious during the initial operation period. The reason for this may be that the cracks in the dam crest have a great influence on the deformation, as shown in Fig. 12. It can be found that there is a long, deep crack in the section of 0 + 240 m found on 26 August 2010. Figure 13 shows the daily range of the water levels of the dam during the operation period. The figure also shows that there is an obvious correlation between the crack development and the water level. The water level is 841.95 m when the first crack is found, and the daily range of the water level is not very fast, with the value of less than 0.4 m/day, but there are obvious rapid rises and falls of water level in the 2–5 months before this time. Additionally, the prediction accuracy of the first half of Fig. 9b is high and occurs before the crack is found. The prediction accuracy of the new method in the second half of Fig. 9b may be affected by the crack, and the influence of water level can be simulated by the HTT model. The analysis results imply that the surrounding environment of the dam has a great effect on the dam deformation during

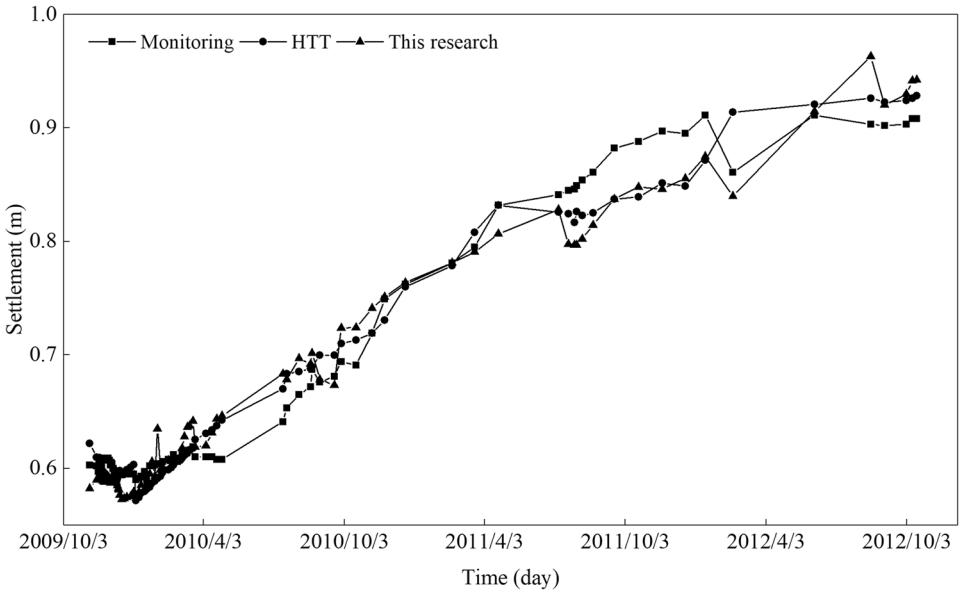

(a) VE1-25

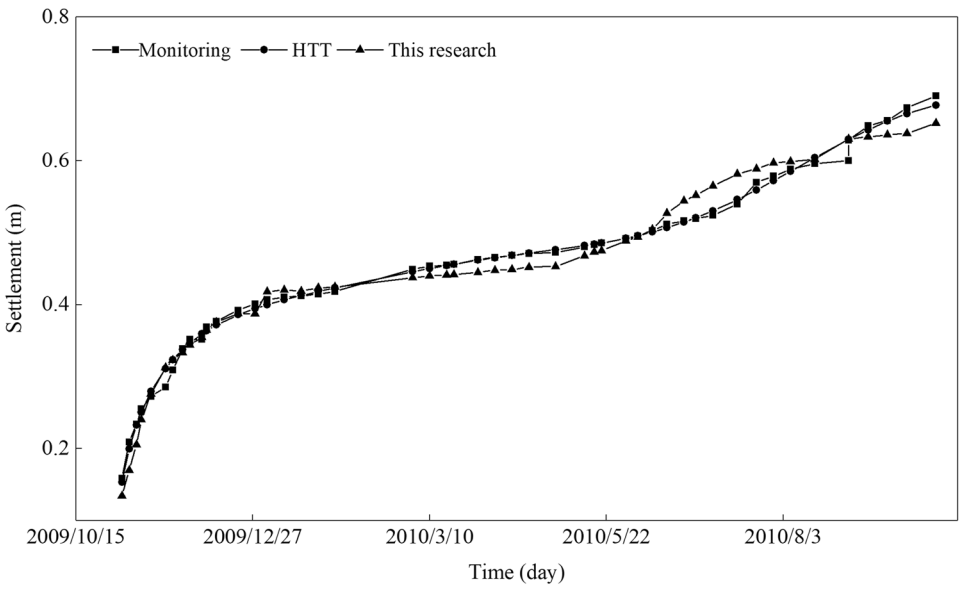

(b) LD 59

Fig. 9 Prediction results for VE1-25 and LD59 during the initial operation period

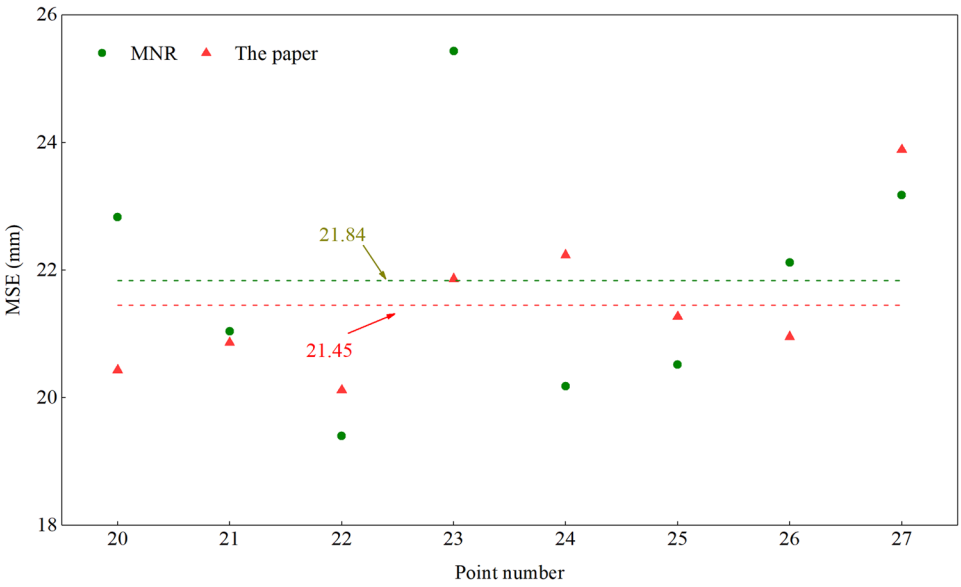

Fig. 10 MSE of results during the initial operation period

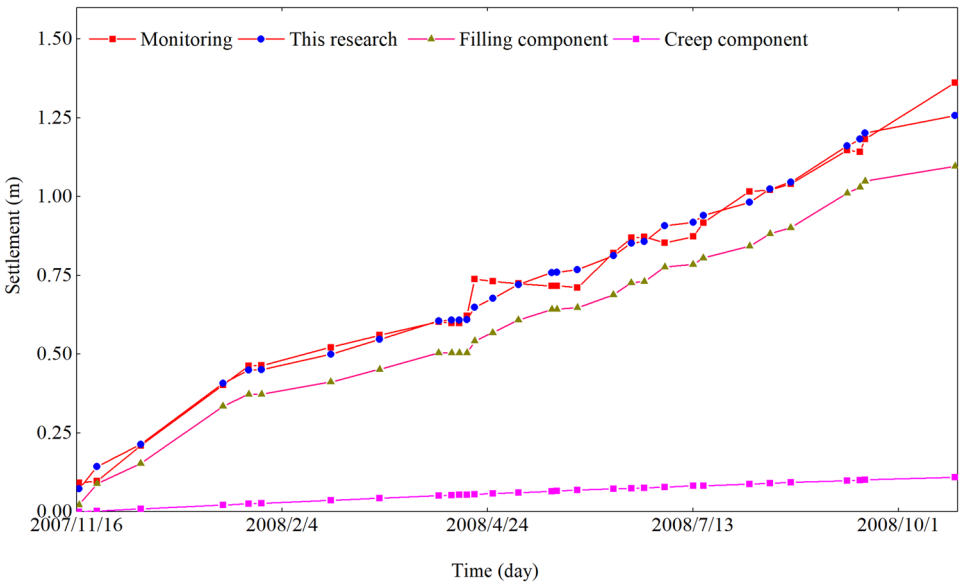

Fig. 11 Filling and creep components of settlement in VE2-36 during the construction period

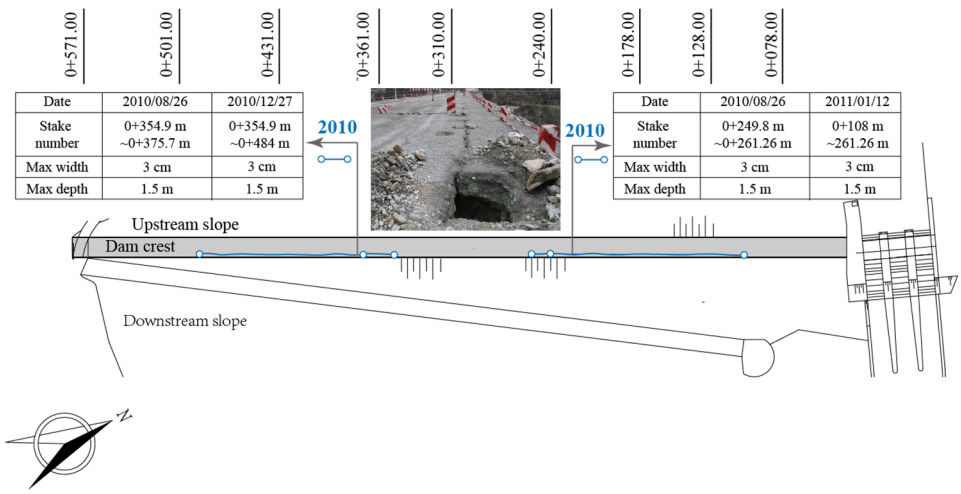

Fig. 12 Development of the crest cracks in the PB dam

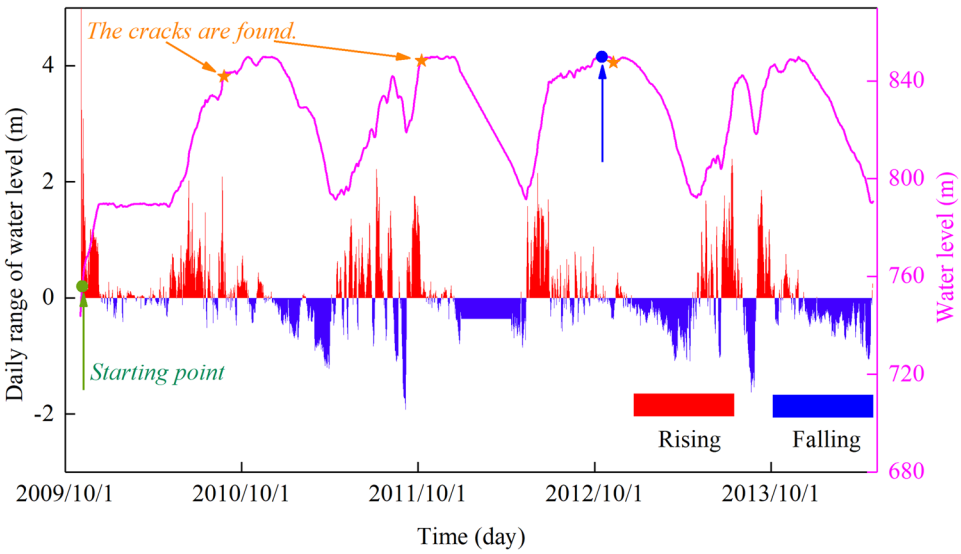

Fig. 13 The water level and the daily range of the dam during the initial operation period

the initial operation period and that the improvement of the accuracy of the model by considering the impact of environmental variables during the operation period needs to be further studied.

In addition, the method proposed in this paper is applicable for core rockfill dams and concrete-faced rockfill dams (CFRDs), and the precondition is to adjust some material parameters correspondingly. For the CFRDs, wetting deformation is not considered during the operation period.

Conclusions

The safety of high rockfill dams has been a research focus worldwide. With the increase of the dam height, the deformation patterns become more complicated. Thus, strengthening the settlement forecasting models of high rockfill dams is of great importance for high-performance prediction targets. In this study, a novel settlement forecasting model is proposed. This model can achieve a successful evaluation of dam deformation during both the construction and operation periods. The factors of the proposed model are determined based on the physical mechanism of dam deformation, which can be used to describe the settlement induced by the dam body and the dam foundation. Additionally, the factors are different due to different causes of settlement deformation during the construction period and initial operation period, and the dam geometric features, complex geological conditions, and different physical and mechanical properties of the materials in the dam body and the foundation are all considered in the promoted model.

The settlement of a rockfill dam during the construction period is made up of immediate settlement and creep settlement. The immediate settlement is defined and derived based on physical causes. The rationality of the model of the immediate compression settlement is verified by a contrastive study using FLAC-3D software. The settlement deformation during the initial operation period includes two parts, the wetting deformation and the unfinished creep deformation, for which the former can be calculated using the modified wetting deformation model of Shen Zhu-jiang.

The proposed novel model is further employed in the PB high rockfill dam in China. The results prove that the new model provides excellent accuracy and agrees well with the monitoring data, and the new model is superior to the traditional regression model in predicting dam settlement in the construction period. The promoted new model expands the theoretical and knowledge of dam settlement prediction and ensures the service safety of high rockfill dams.

Supplementary Information The online version contains supplementary material available at https://doi.org/10.1007/s10064-021-02403-2.

Funding This research was supported by the National Key R&D Program of China (NO. 2018YFC0407103); the National Natural Science Foundation of China (Grant No. 51909181); and the Fundamental Research Funds for the Central Universities.

Declarations

Competing interests The authors declare no competing interests.

References

Alnedawi A, Ai-Ameri R, Nepal K (2019) Neural network-based model for prediction of permanent deformation of unbound granular materials. J Rock Mech Geotech Eng 11(6):1231–1242. https://doi.org/10.1016/j.jrmge.2019.03.005

Behnia D, Ahangari K, Goshtasbi K, Moeinossadat SR, Behnia M (2016) Settlement modeling in central core rockfill dams by new approaches. Int J Min Sci Technol 26(4):703–710. https://doi.org/10.1016/j.ijmst.2016.05.024

Chen X, Lu T, Tan C (2010) Optimization for influence factors of dam displacement base on BP neural network model. Jiangxi Sci 28(1):72–76

Dong W, Yuan H, Xu W, Zhang B, Yu Y (2012) Dynamic back analysis of model parameters of Nuozhadu high core rockfill dam. J Hydroelectr Eng 31(05):203–208

Feng R, He Y, Cao X (2019) Different deformation patterns in high core wall rockfill dams: a case study of the Maoergai and Qiaoqi dams. Adv Civ Eng 2019:7069375. https://doi.org/10.1155/2019/7069375

Feng W, Yin J, Chen W, Tan D, Wu P (2020) A new simplified method for calculating consolidation settlement of multi-layer soft soils with creep under multi-stage ramp loading. Eng Geol 264:105322. https://doi.org/10.1016/j.enggeo.2019.105322

Gu C, Fu X, Shao C, Shi Z, Su H (2020) Application of spatiotemporal hybrid model of deformation in safety monitoring of high arch dams: a case study. J Environ Res Public Health 17(1):319. https://doi.org/10.3390/ijerph17010319

Gurbuz A (2011) A new approximation in determination of vertical displacement behavior of a concrete-faced rockfill dam. Environ Earth Sci 64:883–892. https://doi.org/10.1007/s12665-011-1070-4

Hampel FR (1974) The influence curve and its role in robust estimation. J Am Stat Assoc 69:383–393. https://doi.org/10.2307/2285666

Han B, Geng F, Dai S, Gan G, Liu S, Yao L (2020) Statistically optimized back-propagation neural-network model and its application for deformation monitoring and prediction of concrete-face rockfill dams. J Perform Constr Facil 34(4):0402007. https://doi.org/10.1061/(ASCE)CF.1943-5509.0001485

Herrera G, Fernández-Merodo JA, Mulas J, Pastor M, Luzi G, Monserrat O (2009) A landslide forecasting model using ground based SAR data: the Portalet case study. Eng Geol 105(3–4):220–230. https://doi.org/10.1016/j.enggeo.2009.02.009

Jiang Y, Yan G, Jin W, Suo H, Wang D (2011) Research on foundation seepage control of Luding rockfill dam with clay core wall. Water Power 37(5):17–19

Kan G, Yao C, Li Q, Li Z, Yu Z, Liu Z, Ding L, He X, Liang K (2015) Improving event-based rainfall-runoff simulation using an ensemble artificial neural network-based hybrid data-driven model. Stoch Environ Res Risk Assess 29(5):1345–1370. https://doi.org/10.1007/s00477-015-1040-6

Kim YS, Kim BT (2018) Prediction of relative crest settlement of concrete-faced rockfill dams analyzed using an artificial neural network model. Comput Geotech 35:313–322. https://doi.org/10.1016/j.compgeo.2007.09.006

Lawal A, Kwon S (2021) Application of artificial intelligence to rock mechanics: an overview. J Rock Mech Geotech Eng 13(1):248–266. https://doi.org/10.1016/j.jrmge.2020.05.010

Léger P, Leclerc M (2007) Hydrostatic temperature time-displacement model for concrete dams. J Eng Mech 133(3):267–277. https://doi.org/10.1061/(ASCE)0733-9399(2007)133:3(267)

Li GY, Liu YN (1998) Three-dimensional finite element analysis of the wetting deformation of gravel sand material. In: The Third Young People's Conference of Geotechnical Mechanics and Engineering, Nanjing, 1998

Li G, Mi Z, Fu H, Fang W (2004a) Experimental studies on rheological behaviors of rockfills in concrete faced rockfill dam. Rock Soil Mech 25:1712–1716

Li G, Wang L, Mi Z (2004b) Research on stress-strain behavior of soil core rockfill dam. Chin J Rock Mech Eng 23:1363–1369

Li LG (2009) Analysis of properties and causes of deformation of the Xiaolangdi Hydro Project dam. Adv Sci Technol Water Resour 29(4):39–43

Li M, Wang J (2019) An empirical comparison of multiple linear regression and artificial neural network for concrete dam deformation modelling. Math Probl Eng 2019:7620973. https://doi.org/10.1155/2019/7620948

Li Q, Yu Y, Zhang B, Shen Z (2005) Three-dimensional analysis for the wetting deformation of Gongboxia concrete faced rock-fill dam on the Yellow River. J Hydroelectr Eng 24(3):24–29

Liu Q, Lu G, Dong J (2021) Prediction of landslide displacement with step-like curve using variational mode decomposition and periodic neural network. Bull Eng Geol Environ 80(5):3783–3799. https://doi.org/10.1007/s10064-021-02136-2

Ma H, Chi F (2016) Technical progress on researches for the safety of high concrete-faced rockfill dams. Eng 2(3):332–339. https://doi.org/10.1016/J.ENG.2016.03.010

Macfarlane DF (2009) Observations and predictions of the behaviour of large slow-moving landslides in schist Clyde Dam reservoir New Zealand. Eng Geol 109:5–15. https://doi.org/10.1016/j.enggeo.2009.02.005

Mata J, António T, Costa J (2014) Constructing statistical models for arch dam deformation. Struct Control Health Monit 21(3):423–437. https://doi.org/10.1002/stc.1575

Nie L, Wang H, Xu Y (2017) Application of the arctangent function model in the prediction of ground mining subsidence deformation: a case study from Fushun City Liaoning Province China. Bull Eng Geol Environ 76:1383–1398. https://doi.org/10.1007/s10064-016-0913-3

Niu J, Liang B, Deng Z, Guo Y (2019) Study on nonlinear time-varying statistical model for settlement of high core rockfill dam during construction period. J Nanchang Inst Technol 38(4):1–6

Prakash G, Sadhu A, Narasimhan S, Brehe JM (2018) Initial service life data towards structural health monitoring of a concrete arch dam. Struct Control Health Monit 25(1):e2036. https://doi.org/10.1002/stc.2036

Qian J, Yin Z (1995) Geotechnical Principles and Computations, 2nd edn. Water Resources and Electric Power Press, Beijing

Rashidi M, Haeri S (2017) Evaluation of behaviors of earth and rockfill dams during construction and initial impounding using instrumentation data and numerical modeling. J Rock Mech Geotech Eng 9(4):709–725. https://doi.org/10.1016/j.jrmge.2016.12.003

Salazar F, Morán R, Toledo MÁ, Oñate E (2017) Data-based models for the prediction of dam behavior: a review and some methodological considerations. Arch Comput Methods Eng 24(1):1–21. https://doi.org/10.1007/s11831-015-9157-9

Shen Z (1994) A creep model of rock-fill material and determination of its parameters by back analysis. Hydro-Sci Eng 12(4):335–342

Sortis AD, Paoliani P (2007) Statistical analysis and structural identification in concrete dam monitoring. Eng Struct 29(1):110–120. https://doi.org/10.1016/j.engstruct.2006.04.022

Su H, Li X, Yang B, Wen Z (2018) Wavelet support vector machine-based prediction model of dam deformation. Mech Syst Signal Process 110:412–427. https://doi.org/10.1016/j.ymssp.2018.03.022

Tang T, Li G, Xu Z (2001) Statistic prediction models of settlement for earth-rock dam. Hydro-Sci Eng 3:29–34

Tasci L, Kose E (2016) Deformation forecasting based on multi-variable grey prediction models. J Grey Syst 28:56–64. https://doi.org/10.1108/GS-04-2019-0007

Tomás R, Cano M, García-Barba J, Vicente F, Herrera G, Lopez-Sanchez JM, Mallorquí J (2013) Monitoring an earthfill dam using differential sar interferometry: La Pedrera dam Alicante Spain. Eng Geol 157:21–32. https://doi.org/10.1016/j.enggeo.2013.01.022

Wan Y, He Y (2016) Seismic response law of cutoff wall of Huangjinping rockfill dam. Eng J Wuhan Univ 49(3):378–383. https://doi.org/10.14188/j.1671-8844.2016-03-010

Wang W, Höeg K, Zhang Y (2010) Design and performance of the Yele asphalt-core rockfill dam. Can Geotech J 47(12):1365–1381. https://doi.org/10.1139/T10-028

Wu W, Shui S (2019) Analysis of safety monitoring data of Changheba extra high earth rock dam during the first impoundment period. Des Hydroelectr Power Station 35(2):90–93

Xiang J, Hu Z (2016) Construction technology of cut-off wall for measuring weir of Houziyan Hydropower Station in Sichuan. Hong-Shui River 35(2):34–36

Xue S, Lv J, Pang B (2012) Treatment of deep thick cover layer of dam foundation of Pubugou Hydropower Station. Yangtze River 43(4):35–38

Yao Y, Li S, Zhang B (2011) Application of stepwise regression-PLS model to dam displacement monitoring. Water Res Power 29(4):81–82

Yu D, Ye J, Yao L (2020) Prediction of the long-term settlement of the structures built on a reclaimed coral reef island: an aircraft runway. Bull Eng Geol Environ 79:4549–4564. https://doi.org/10.1007/s10064-020-01866-z

Yu H, Wu Z, Bao T, Zhang L (2010) Multivariate analysis in dam monitoring data with PCA. Sci China Technol Sci 53:1088–1097

Zhang H, Chen J, Hu S, Xiao Y, Zeng B (2016) Deformation characteristics and control techniques at the Shiziping earth core rockfill dam. J Geotech Geoenviron Eng 142(2):04015069. https://doi.org/10.1061/(ASCE)GT.1943-5606.0001385

Zhang W, Xiao R, Shi B, Zhu H, Sun Y (2019) Forecasting slope deformation field using correlated grey model updated with time correction factor and background value optimization. Eng Geol 260:s105215. https://doi.org/10.1016/j.enggeo.2019.105215

Zhu P, Zhou W (2010) Characteristics of Shuiniujia Hydropower Station. Sichuan Water Power 29(6):80–84

Zou J, Bui KT, Xiao Y, Doan C (2018) Dam deformation analysis based on BPNN merging models. Geo Spat Inf Sci 21(2):149–157. https://doi.org/10.1080/10095020.2017.1386848